Seismic evidence for a deeply rooted low-velocity anomaly in the upper mantle beneath the northeastern Afro/Arabian continent

Eric Debayle, Jean-Jacques Lévêque *, Michel Cara

IPGS - Ecole et Observatoire des Sciences de la Terre, CNRS and Université Louis Pasteur, 5 rue René Descartes, 67084 Strasbourg, France

Abstract

We present seismic results that support the presence of a small, low shear velocity anomaly deeply rooted in the upper mantle transition zone beneath southern Arabia and the Red Sea. The low shear velocity anomaly persists down to the 660 km discontinuity. It is found from the waveform inversion of 2741 Rayleigh wave seismograms taking into account several higher modes. We use records from the permanent IRIS and GEOSCOPE stations completed with data collected after various field deployments of portable stations in the Horn of Africa (INSU experiment), Tanzania, Saudi Arabia and Tibet (PASSCAL experiments). The complete dataset provides a dense ray coverage of the Afro/Arabian continent and allows shear-wave heterogeneities to be resolved with wavelengths of a few hundred kilometers. To achieve a good vertical resolution in the whole upper mantle, we analyze up to the fourth Rayleigh mode in the period range 50–80 s, in addition to the fundamental Rayleigh mode in the period range 50–160 s. We discuss whether the pattern of upper mantle shear velocity anomaly could be related to local causes or to one or several plume conduits in the region. Our lateral resolution may intuitively not be sufficient to resolve a narrow plume conduit at transition zone depths. However, we show that when a dense coverage is available, a narrow low-velocity anomaly will affect the path-average measurements for a large number of individual seismograms crossing the anomaly. In this case, the low-velocity perturbation is mapped in the tomographic model, even though smoothed by the lateral resolution. We conclude that our observation is difficult to attribute to a shallow origin or to reconcile with a single narrow plume conduit in the region. It can be explained either by several close narrow plume tails or by a broad region of upwelling. © 2001 Elsevier Science B.V. All rights reserved.

Keywords: upper mantle; Afar Depression; plumes; surface waves; tomography

1. Introduction

The Afar and surrounding regions, which include the Ethiopian plateau, the Red Sea and western/southern Arabia have been affected by several geodynamical processes involving rifting, uplift and magmatism. Geochemical and geolog-

———

* Corresponding author.

E-mail addresses: eric@sismo.u-strasbg.fr (E. Debayle), leveque@sismo.u-strasbg.fr (J.-J. Lévêque).

ical evidences [1] suggest that two periods of tectonic activity played a major role in shaping the region to its current form.

A first period of uplift, rifting and magmatism has been identified in the late Oligocene and early Miocene (from about 30 to 20 Ma) and is contemporaneous with the opening of the Red Sea and Gulf of Aden rifts. These oceanic rifts could have been initiated by tectonically induced extension involving a passive mantle (see e.g. [2]). Voluminous trap series basalts erupted in Yemen and Ethiopia are contemporaneous of this period [1,3].

A second major period of uplift began in the mid-Miocene (14 Ma) and has continued to the present. We know from fission track data that the rate of uplift was accelerated after 14 Ma but it may have been initiated as early as 20 Ma [4]. Contemporaneous magmatism has been observed in western Saudi Arabia [1] and could be related to the upwelling of hot asthenosphere. These evidences support the idea that a thermal plume has been active a long time after the initial breakup of the continental lithosphere and may still be present beneath the region.

Seismic observations in the uppermost 200 km of the mantle are compatible with a thermal plume model. At sublithospheric depths, the plume conduit is expected to spread out at the bottom of the lithosphere and to produce a broad low-velocity perturbation. Surface observations and laboratory experiments (see e.g. [5]) suggest that the size of the uplifted region at the surface may reflect the low-velocity anomaly. The Afro-Arabian dome covers a broad region including the Afar, the Ethiopian plateau, Eritrea, Yemen and the western part of Saudi Arabia [1,6]. Its northern part corresponds to a region of late Tertiary uplift, the west Arabian swell, which is about 1200 km wide. The entire region is underlain by a broad low-velocity anomaly in tomographic models (see e.g. [7,8]). At regional scale, Knox et al. [9] found seismic velocities 0.2–0.8 km/s lower than PREM at 100 km depth beneath the Afar and western Saudi Arabia.

At transition zone depths, numerical modelling, theoretical predictions and laboratory experiments suggest that the plume conduit should be a narrower structure, with a diameter ranging from about 50 to 600 km [5,10–13]. Because deep objects with small lateral extension remain difficult to image with seismological techniques, there is to our knowledge no seismic observations at transition zone depths to support a plume model in the upper mantle beneath the region. Recently, Nyblade et al. [14] found a transition zone thickness beneath Afar consistent with the global average. They conclude that a broad thermal anomaly beneath Afar may not extend as far down as the transition zone, although a shear velocity perturbation smaller than 1%, consistent with a 100–150 K thermal perturbation cannot be ruled out.

In this paper we present results from a surface wave tomography of fundamental and higher mode Rayleigh waves that support the presence of a small low-velocity anomaly deeply rooted in the upper mantle beneath the Red Sea and southwestern Arabia. The anomaly persists with a small amplitude at transition zone depths down to the 660 km discontinuity. A good vertical resolution is obtained in the whole upper mantle beneath the region thanks to the use of higher Rayleigh modes. The lateral resolution is about a few hundred kilometers. At first glance, it may intuitively not be sufficient to resolve a narrow plume conduit. However, we show that when a dense coverage is available, a narrow low-velocity anomaly will affect the path-average measurements for a large number of individual seismograms crossing the anomaly. In this case, the low-velocity perturbation is mapped in the tomographic model even though smoothed by the lateral resolution, and thus can be detected.

2. Region under study

We analyze Rayleigh wave seismograms recorded at regional distances, in a region that covers the eastern part of Africa, the southern part of Asia and the northern Indian Ocean (Fig. 1). The data have been recorded at the permanent IRIS and GEOSCOPE stations available in the region, supplemented by temporary stations deployed in the field. In the Horn of Africa region, the French 'Institut National des Sciences de l'Univers'
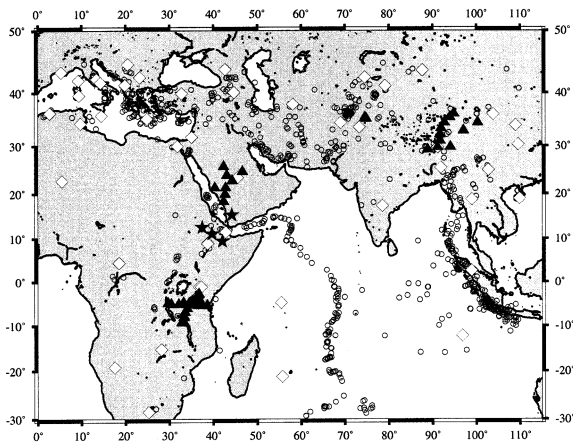
Fig. 1. Station and epicenter locations. Permanent stations from the IRIS and GEOSCOPE networks are shown with white diamonds. Portable broad-band stations from the INSU and PASSCAL experiments are shown with black stars and triangles, respectively. Epicenters are plotted as open circles. (Figure produced using the GMT software [44].)

(INSU) started in June 1999 the installation of four broad-band stations equipped with STS2 seismometers. Three of these stations have been deployed in Ethiopia while the last one is installed in Yemen (Fig. 1). This regional network provides us with useful additional ray coverage in northeast Africa and southern Arabia, especially for short epicenter–station paths corresponding to regional events. Other data collected on the field come from the PASSCAL experiments in Tanzania, Saudi Arabia and Tibet.

3. Building a three-dimensional (3D) model

3.1. Tomographic procedure

The construction of a 3D model of upper mantle shear-wavespeed variation is achieved from a two-step technique that has previously been applied successfully to regional studies of the Indian Ocean [15] and Australia [16,17].

In a first step, the waveform inversion technique of Cara and Lévêque [18] produces a path-average 1D upper mantle model that represents the waveform of a Rayleigh wave seismogram recorded for a given epicenter–station

path. The technique has recently been automated and allows an efficient analysis of large dataset [19].

The 1D models obtained for the set of epicenter–station paths are then combined in a tomographic inversion using the continuous regionalization algorithm of Montagner [20]. The technique allows us to consider both azimuthal anisotropy and isotropic lateral variations of shear velocity in the inversion. In this paper, we only discuss the lateral variations of the shear-wave velocity. Seismic anisotropy beneath northeastern Africa and Saudi Arabia has been studied using both surface [21] and body-waves [22,23]. Hadiouche et al. [21] found a relatively weak zone of SV wave azimuthal anisotropy, down to 88 km depth, beneath northeastern Africa. Typical SKS delay time between 1 and 1.5 s have been obtained in the Afar [23] or Saudi Arabia [22]. These measurements are consistent with a relatively shallow seismic anisotropy located in the upper 200 km of the mantle. Using our own dataset, we performed different styles of inversion, with and without anisotropy. In agreement with previous studies, our results suggest that a small percent of azimuthal anisotropy are present down to 150–200 km depth beneath northeastern Africa while at larger depths, seismic anisotropy can be neglected. In the upper 200 km, a small trade-off is observed between the isotropic and the anisotropic components of the model, but with an amplitude that is too small to change the pattern of seismic heterogeneities. In the transition zone, the result of our tomographic inversion is very stable, whether anisotropy is included or not in the inversion. Artifacts due to trade-off between anisotropy and lateral heterogeneities [24] are thus very unlikely in the results we display here.

In the following, we only present the isotropic part of the shear-wave velocity model. Interpretation of the anisotropic part of the model would need much more development and is out of the scope of this paper.

3.2. Waveform analysis

The waveform inversion technique has been designed to process the fundamental mode and few

overtones of the surface waves. In this study, we work in the period range 50–160 s and we process the fundamental and up to four higher Rayleigh modes, depending on their signal-to-noise ratio, using an automated procedure designed to process a large number of seismograms [19]. The inversion is performed for the upper mantle structure only, assuming that the crustal structure is known.

Restricting the analysis to 50 s for the shortest periods allows us to avoid problems due to strong lateral variations in the shallow Earth layers, especially in parts of the model where strong crustal variations are expected. For epicenter–station paths smaller than 10 000 km, it is widely accepted that the great-circle approximation used in this study is reasonable at 50 s of period (see e.g. [25] or [26]) even for the fundamental mode whose sensitivity is confined in the uppermost layers of the mantle. In addition, because the maximum sensitivity of the fundamental mode at 50 s of period is located at 70 km depth (Fig. 2), well below the crust, we determine seismic velocities from a dataset primarily sensitive to the upper mantle.

We nevertheless perform crustal corrections using the 3D representation of the crustal structure provided by the 3SMAC model of Nataf and Ricard [27]. As shown in Section 4, comparisons with other tomographic results where shallow layer corrections are based on a different crustal model suggest that for the period range of analysis the 3SMAC corrections allow minimization of the biases due to an imperfect knowledge of the crust.

The number of higher modes considered in the inversion has been chosen to allow resolution at transition zone depths while minimizing possible artifacts due to approximations made in the theory. Considering independent perturbation of each mode branch, the four overtones used here in the period range between 50 and 80 s provide sensitivity in the mantle down to at least 700 km depth (Fig. 2). Artifacts have been shown to be present at transition zone depths when long period body phases are matched without considering the mode coupling [28]. Indeed, multiple reflected body-wave phases are sensitive to model perturbations close to their geometrical ray rather than to the horizontally averaged model perturbation used in the path-average approximation. However, we use a time window that corresponds to a limited number of higher modes at periods larger than 50 s. In this period range and time window, the modes are well separated so that neglecting their coupling in the inversion should not significantly bias our results. The previous global study by Ritsema et al. [8] was based on a similar number of surface wave higher modes used in the same frequency range of analysis. Their results, also obtained without mode coupling, provided high vertical resolution in the transition zone.

In this study, we have analyzed the waveforms of 2741 Rayleigh wave seismograms. The fundamental mode has been considered in the inversion for 2732 seismograms while for 2006 paths, at least one overtone was taken into account in the inversion (Fig. 3).
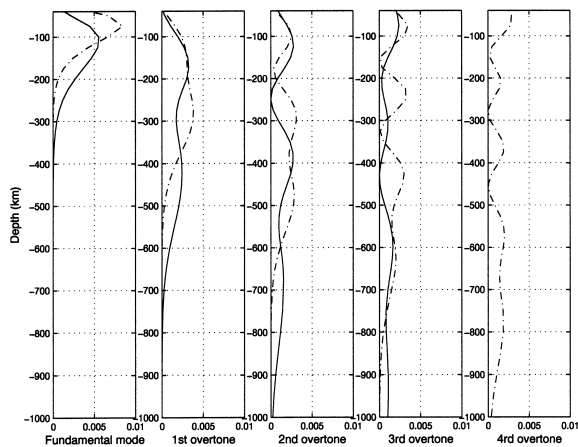

Fig. 2. Sensitivity kernels for the fundamental and up to the fourth higher mode of Rayleigh waves. The curves represent the relative partial derivatives of the phase velocity according to the shear-wave velocity (V_{sv}/C)($\delta C/\delta V_{sv}$). These partial derivatives are shown for a 1 km thick layer, at periods of 50 s (dash–dot line) and 80 s (continuous line).

4. Tomographic images

The uppermost part of our tomographic model is presented in Fig. 4. Lateral variations in shear velocity are plotted at 100 and 200 km depth. In
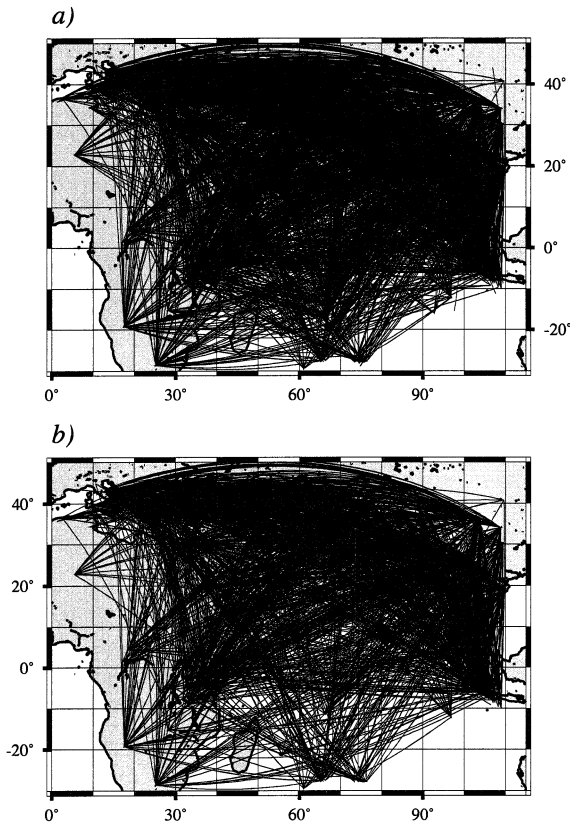
Fig. 3. Actual path coverage corresponding to: (a) data for which the fundamental modes have been taken into account in the inversion, (b) data for which the higher modes have been taken into account. A total of 2741 Rayleigh wave seismograms have been analyzed.

this depth interval, we retrieve the well-known correlation with surface tectonics.

In the northern Indian Ocean, mid-oceanic ridges have a rather shallow low-velocity signature, suggesting that vertical smearing of shallow seismic anomalies is weak. The dominant seismic anomaly at 200 km depth is a slow perturbation shifted westward of the Central Indian ridge. In southeast Asia, the Tibetan plateau is underlain by a low-velocity layer which extends down to about 120 km depth. At larger depths, the long wavelength S-wave structure is dominated by high seismic velocities. These observations agree with recent surface wave tomographic models for the upper mantle of the Indian Ocean [15,29] and southeast Asia [30].

In eastern Africa, our shear velocity maps can be compared with the global model S20RTS of Ritsema et al. [8] or with the regional model of Ritsema and van Heijst [29]. Ritsema et al. [8] used a global dataset of fundamental, higher modes and body-waves to constrain the structure down to the lower mantle. However, the lateral resolution in this global study is not better than 2000 km. Our regional model includes shorter paths and provides a much better horizontal res-
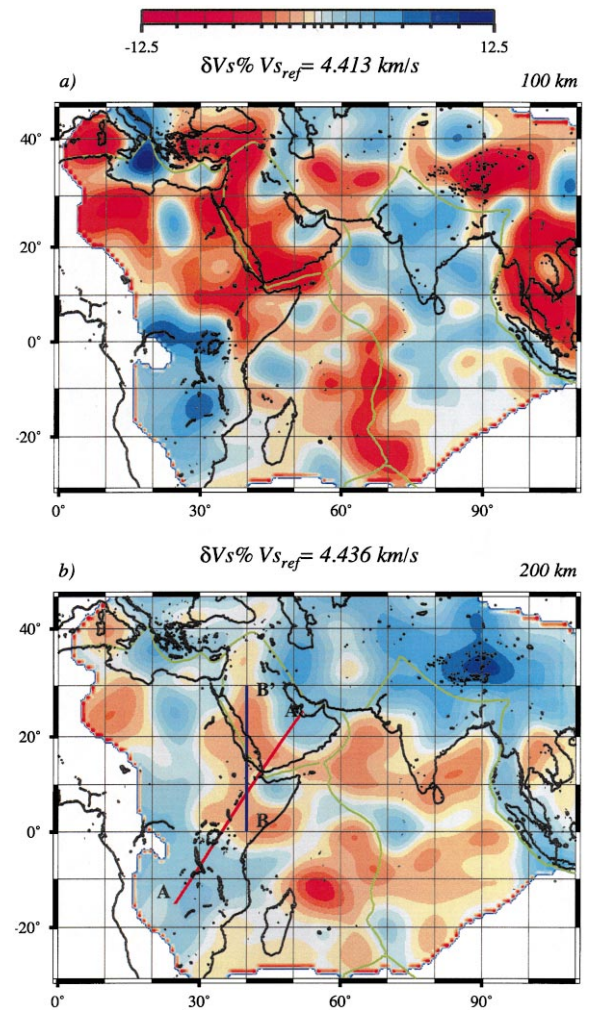

Fig. 4. SV wave heterogeneities at 100 km depth (top) and 200 km depth (bottom). Cross-sections AA' and BB' of Fig. 5 are indicated on the map.

olution of a few hundred kilometers (see Section 5). It is, from this point of view, closer to the regional work of Ritsema and van Heijst [29]. These authors achieved a dense coverage of the African continent through the analysis of about 8000 fundamental Rayleigh modes in the period range between 40 and 200 s. They used the CRUST5.1 model derived by Mooney et al. [31] to perform crustal corrections. Their inversion results in a 3D shear velocity model for the uppermost 400 km of the mantle. For comparison, our dataset provides a dense coverage of the African continent only eastward of 30°E but our analysis includes higher modes and a better resolution is expected at transition zone depths. We also perform crustal corrections using the 3SMAC model of Nataf and Ricard [27] instead of CRUST5.1. Despite these differences in data selection and a priori assumptions, the distribution of seismic anomalies agrees well for the uppermost 250 km of the mantle beneath the eastern part of Africa where both studies are expected to provide good resolution. In the Afar and surrounding regions, a broad low-velocity anomaly is found at 100 km depth, with a maximum low-velocity perturbation located beneath Yemen, western Saudi Arabia and the Ethiopian plateau. A sharp transition from low to high velocities characterizes in both studies the boundary between the Ethiopian plateau and the southern Tanzania craton.

At larger depths, a small low-velocity anomaly persists down to 300 km depth beneath the Ethiopian plateau in the Ritsema and van Heijst [29] model. We display in Fig. 5 two vertical sections along great-circle paths that cross eastern Africa. Both sections suggest that a small low-velocity anomaly extends down to 400 km depth beneath the Ethiopian plateau, slightly deeper than in the Ritsema and van Heijst [29] model. At larger depths, the low-velocity anomaly beneath the Ethiopian plateau vanishes (Fig. 5). However, north of the Ethiopian plateau, a low-velocity anomaly elongated in the east–west direction from the western coast of the Red Sea to southern Arabia persist down to a depth of 650 km (Figs. 5 and 6).

In the two following sections, we discuss the robustness of this more deeply rooted low-velocity anomaly, and its implication in terms of upwelling material beneath the region.
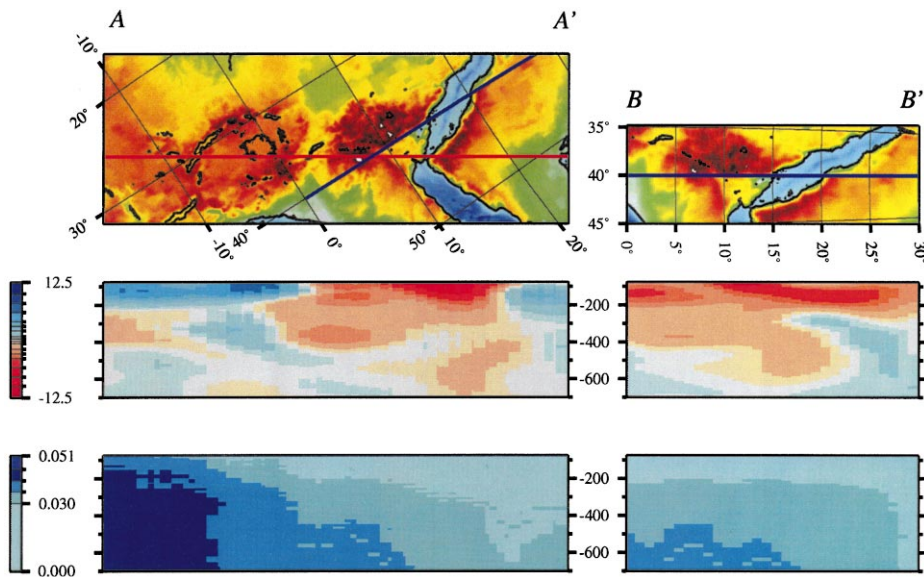

Fig. 5. Vertical cross-sections for the great circles AA′ (left) and BB′ (right). The cross-sections start at 75 km depth and are represented through the SV velocity model and the a posteriori error distribution (bottom). Cross-section locations and topography are shown on top.
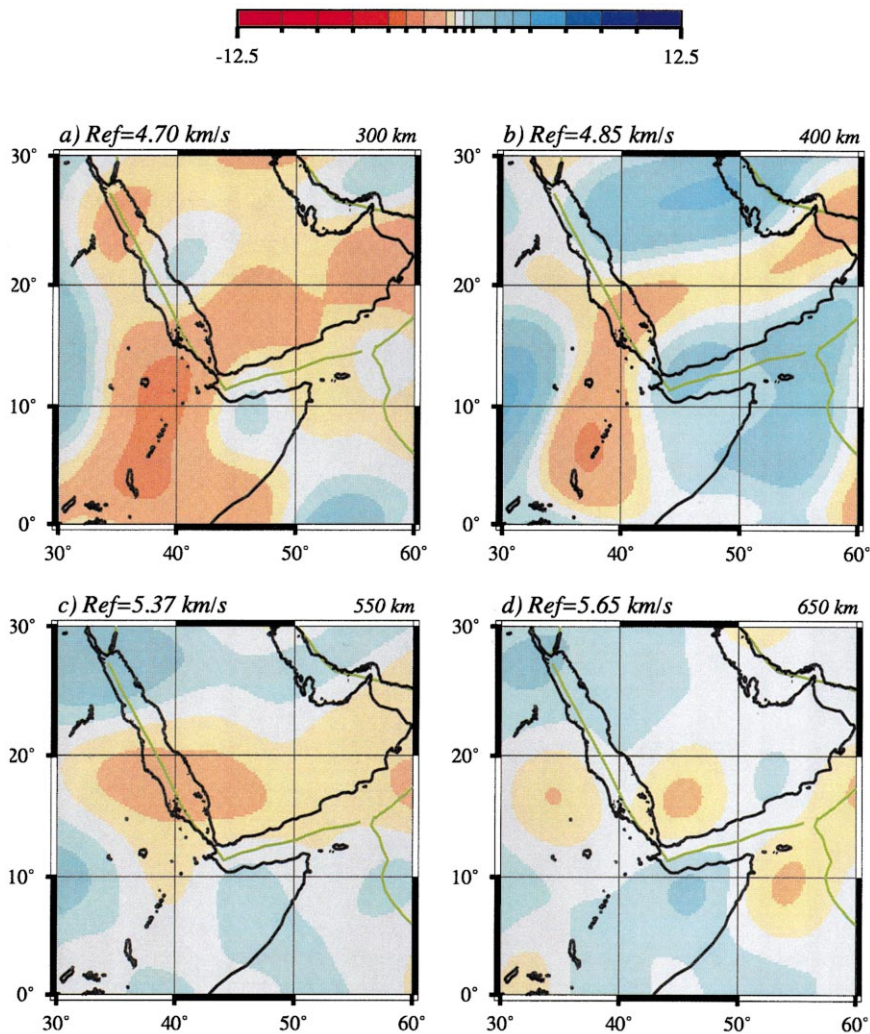
Fig. 6. SV wave heterogeneities beneath the Horn of Africa for the deeper part of the model.

5. Reliability of the model and resolution tests

The construction of our 3D shear-wavespeed model results from a two-step process. The first step is equivalent to interpreting the dispersion of the different modes present in each individual seismogram in terms of a 1D depth-dependent shear velocity model. The second step allows us to retrieve lateral variations in shear velocity by combining, at each depth, the shear velocity slowness values obtained for each epicenter–station path.

There are many effects that can produce arti-facts on the 1D path-average velocity models. These include effects due to the approximation used in the theory or too poor a knowledge of non-inverted parameters such as the crustal structure along the path and the focal mechanism at the source.

As discussed in Section 3.2, the great-circle approximation is likely to be valid in our frequency band of analysis for relatively short paths and the neglect of mode coupling should not affect our results. The use of the 3SMAC crust has also been shown to allow a reliable estimation of the
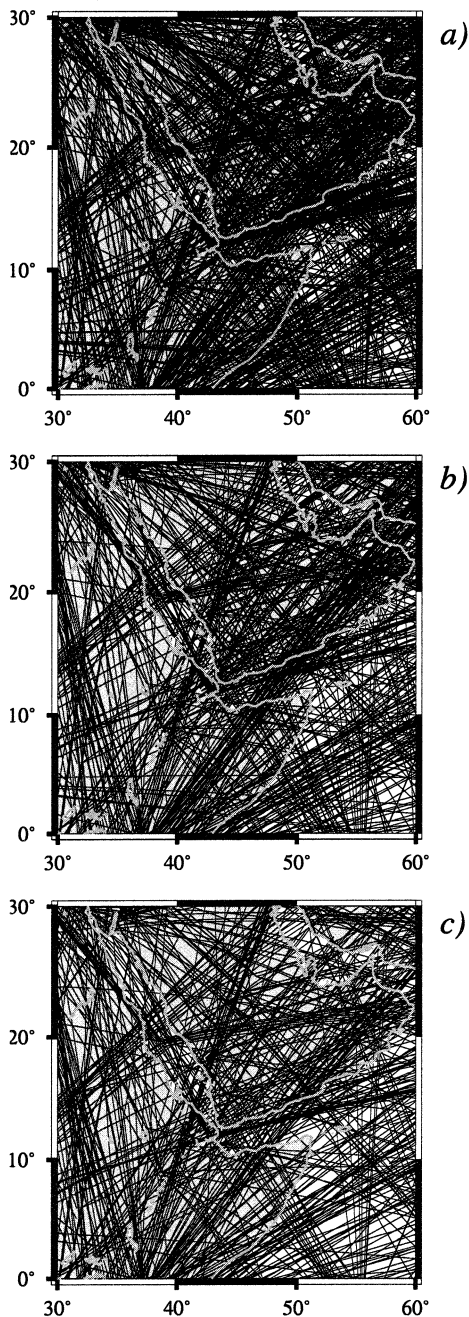
Fig. 7. Path coverage in fundamental and higher modes for the region of interest. (a) Fundamental and first overtone; (b) second and third overtone; (c) fourth overtone.

structure in the uppermost 200 km of the mantle, mostly constrained by the fundamental Rayleigh mode. At greater depths the structure is mostly constrained by long-period higher modes less sensitive to shallow layers. Therefore, crustal corrections are not expected to produce significant artifacts at transition zone depths. Errors in the source parameters may bias the path-average shear velocity estimation for some of the 1D models. However, the paths for which this bias is strong are rejected by applying the selection criteria. For paths less biased that could pass the rejection tests, these effects have no reason to be coherent since they are related to earthquakes with different focal mechanisms or different focal depths. Therefore, they should be averaged out in the tomographic inversion if a large number of paths with different azimuths is used to constrain the structure. We present in Fig. 7 the distribution of rays crossing northeast Africa and southern Arabia for data subsets corresponding to different Rayleigh modes, thus sampling different depths intervals of the upper mantle. For our period range of analysis, the fundamental and first overtone (Fig. 7a) allow us to constrain the uppermost 400 km of the mantle (see Fig. 2). The second and third overtones (Fig. 7b) provide sensitivity down to 700 km while the fourth overtone (Fig. 7c) provides additional coverage in the whole depth of inversion. Each depth interval is constrained by a large number of criss-crossing rays, related to different types of sources (mid-oceanic ridges in the Indian Ocean, subduction zone in Greece, continental rift in east Africa and continental collision between Africa and Eurasia or India and Asia). It is thus reasonable to assume that possible artifacts due to source effects are averaged out at each depth owing to our ray coverage.

We would now like to discuss the reliability of our results in both the depth location of the anomaly and its horizontal extent. In a first experiment, we fully test how a very simple model is smeared horizontally and vertically. For this purpose, we put a −5% shear-wave velocity anomaly over a rectangular box 400 km wide in the north–south direction, 1000 km wide in the east–west direction, and 150 km high. The anomaly is located beneath the Red Sea at depths between 300
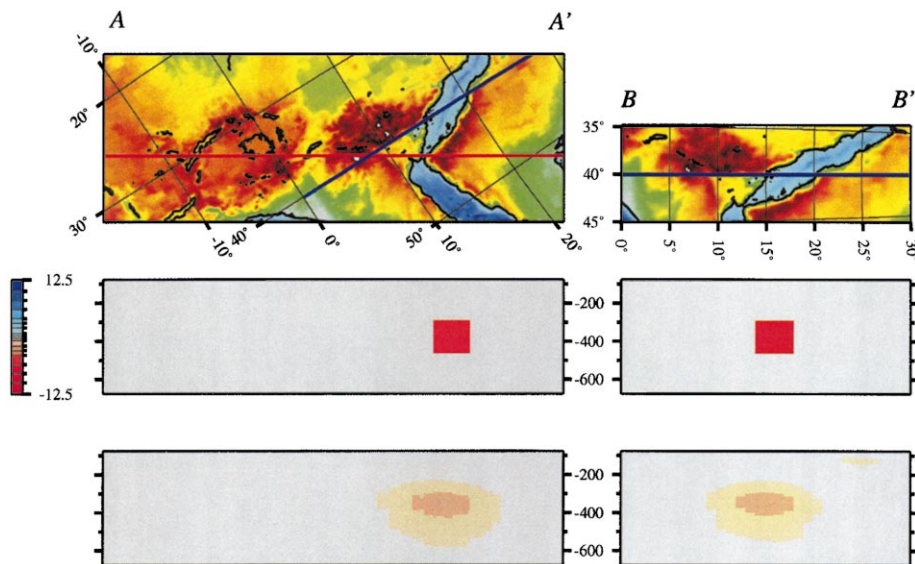
Fig. 8. Synthetic experiment to test vertical and horizontal smearing in the transition zone. Cross-sections are the same as in Fig. 5. A −5% shear velocity perturbation with a 400×1000 km horizontal extension has been added to a smooth PREM model between 300 and 450 km depth (upper cross-sections). The synthetic experiment reproduces the two steps of our tomographic procedure, i.e. the automated individual analysis of 2741 synthetic waveforms computed for each path of the study (1D inversion) followed by a linear tomographic inversion allowing us to obtain the 3D structure. Each stage of the inversion is carried out under the same conditions as the actual inversion. The output of the inversion, presented on the bottom cross-sections, demonstrates that our fundamental and higher mode dataset allows us to isolate a low-velocity anomaly in the transition zone.

and 450 km (Fig. 8). The embedding structure is a PREM mantle overlain by the 3SMAC crustal model. For each path of our study, a synthetic seismogram is computed for waves propagating in the average structure along the path. The set of 2741 synthetic seismograms is then inverted following the same automated procedure as for actual data. The 3D model we obtain as the result of the tomographic inversion is displayed on Fig. 8 along the same cross-sections we use for Fig. 4. It is clear from this experiment that the initial anomaly is smoothed over a larger region. However, the vertical smearing remains small. No anomaly is found at shallow depths (< 200 km) nor at great depths (> 550 km), thus indicating that depth location of anomalies found from inversion of actual data is likely to be correct. In the horizontal direction, the amount of spreading is a little bit larger but again, the location of the retrieved anomaly is roughly correct.

In a second experiment, we intend to mimic more closely what could happen to a narrow plume when viewed through our tomographic method. Since the anomaly to be retrieved is now much smaller in the horizontal direction, we concentrate our efforts on the study of the horizontal spreading of such an object. For sake of simplification and computer-time saving, we do not come back to the synthetic seismograms, we instead restrain the computations to the path-average S-velocity models. This simplification does not impair at all the estimation of horizontal resolution. It only degrades the estimation of vertical resolution. However, this is no longer a concern since we have already studied it in the first synthetic experiment.

In this second experiment, we illustrate how a small-scale anomaly with −5% over 200 km width, once recorded in the 1D models, is mapped in the 3D model through the tomographic inversion. The 1D path-average shear velocity models are first determined by integrating the input model slowness along the great-circle paths corresponding to our path coverage. The tomographic inversion is then performed with the same a priori values in the data and the model as in the actual

inversion. In particular, the weight given at each depth to each 1D path-average model depends on its a posteriori error determined after the actual waveform inversion. This a posteriori error is large at a given depth when the actual waveform contains little information related to the corresponding structure. In this way, our synthetic ex-

periment carries the depth sensitivity of the actual dataset.

Fig. 9 shows that under the conditions of our experiment, even a narrow plume conduit is mapped in the 3D model once it has been recorded in the path-average shear velocity model. The narrow structure is smoothed by the tomo-
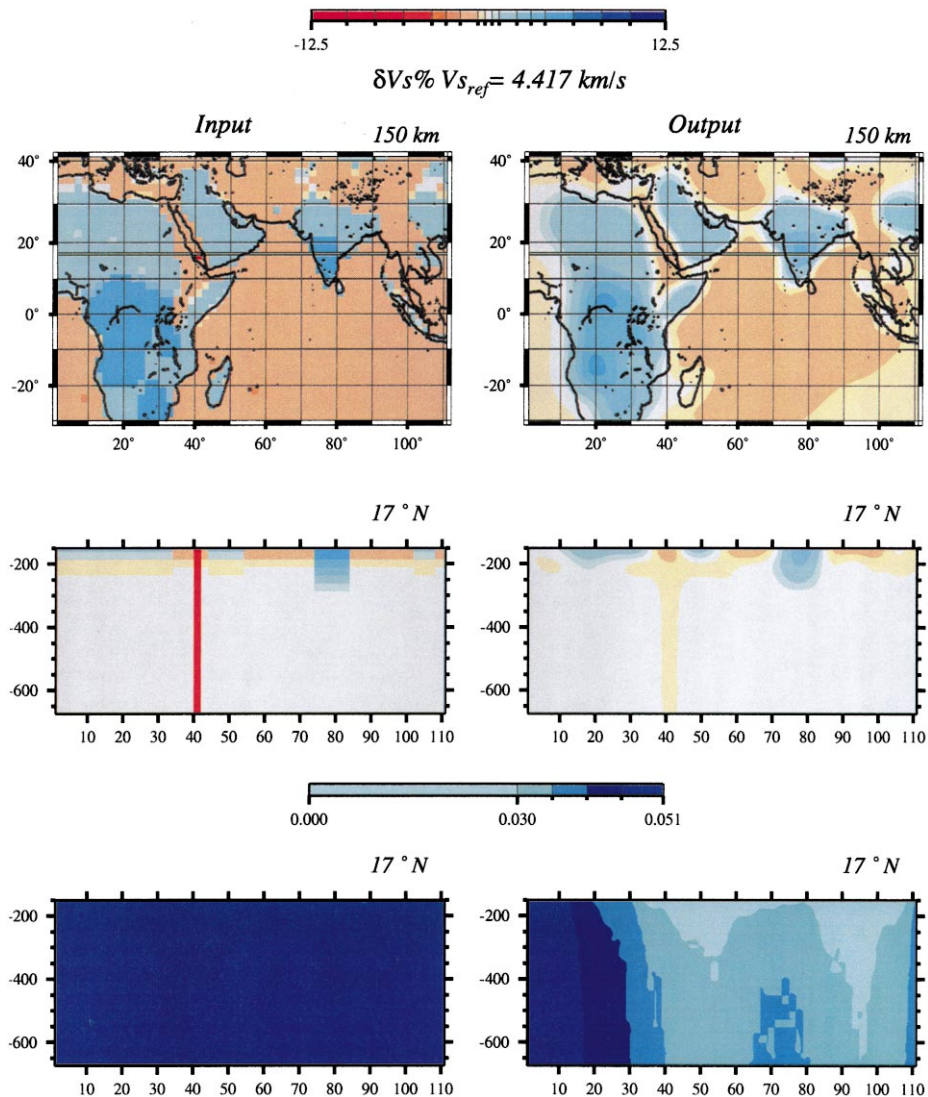

Fig. 9. Synthetic experiment carried out under the same conditions as the actual inversion. The input Earth model (left column, top and middle) is the 3SMAC model of [27] with a −5% shear velocity perturbation added in a narrow conduit located at latitude = 17°N and longitude = 43°E. The conduit is about 200 km wide and extends down to a depth of 700 km. Output of the inversion is represented on the right column. A priori (left column) and a posteriori (right column) errors on the model parameters are displayed at the bottom of the figure. The a priori error for the 3D model is uniform and set to a value of 0.05 km/s in the tomographic inversion.

graphic inversion and the output is a strongly attenuated low-velocity anomaly with a diameter of about 400 km, corresponding to the horizontal degree of smoothing imposed in the inversion. This synthetic test also shows that the amplitude of the fast velocity anomaly located at 80°N, whose lateral extent is broader and exceeds the horizontal degree of smoothing, is well restituted. As expected, the final a posteriori error (right column, bottom of Fig. 9) on the 3D model is small in those parts of the model where a good resolution is achieved, which is the case for northeastern Africa and the Arabian plate. It is equal to the a priori error (left column of Fig. 9) when the resolution is null, mainly on the edges of the cross-section.

The low-velocity anomaly observed in the model after inversion of the actual dataset (Fig. 5) has an amplitude slightly larger than the a posteriori error in this part of the model. It extends to depths of about 400 km beneath the Ethiopian Plateau and deeper, down to the 660 km discontinuity beneath the Red Sea and southern Arabia. It appears as a relatively broad structure, even in the transition zone where it is elongated in the east–west direction.

6. Discussion

It has been suggested that the lithosphere and shallow upper mantle may exert strong control on the location of seismic and geochemical anomalies observed beneath hotspots and continental flood basalts [32,33], especially near pre-existing rifts. However, although a role of the lithosphere and upper mantle cannot be ruled out in explaining the shallower part of our observed seismic anomaly, we will see that its depth extension suggests other processes responsible for the upwelling of deeper materials.

Local convection confined to the upper mantle could occur at the border between the Tanzania craton and the Ethiopian plateau. Indeed, cross-section AA′ of Fig. 5 exhibits a strong S-velocity contrast at lithospheric depths indicating a large horizontal temperature gradient. In a similar situation, a 2D numerical modelling of upper mantle

convection at the oceanic border of a craton [34] shows that local instability of the upper mantle may be generated. Cold material is expected to sink beneath the craton. It may even penetrate through the 410 km discontinuity while hot material rises beneath the adjacent hot and young oceanic lithosphere. This scheme may be in qualitative agreement with what we observe in the central part of cross-section AA′, at the border between the Tanzania craton and the Ethiopian plateau. As an alternative to a plume model, the broad low-velocity anomaly extending from the surface to 400 km beneath the Ethiopian plateau might thus have a local cause.

Beneath the Red Sea, it seems difficult to invoke a similar destabilization of the base of the Saudi Arabian proterozoic lithosphere to explain the low-velocity anomaly we observe in the transition zone (Fig. 6c and cross-sections of Fig. 5). A downward flow of cold material is not observed in our tomographic model and a much stronger local instability would be required to generate an upwelling flow deeply rooted in the transition zone. It is thus very likely that this deep low-velocity anomaly has another origin.

As discussed previously, the horizontal resolution available with long period surface waves does not allow us to address in detail the geometry of this low-velocity structure in the transition zone. Its elongated shape and lateral extent (about 1000×500 km at 550 km depth on Fig. 6c) suggests that it has been created by a structure more complex than a simple narrow plume conduit. A 1000 km wide region of upwelling, or few close narrow plume conduits could as well explain the pattern of low-velocity anomaly we observe.

A broad region of upwelling is at first glance not easy to reconcile with laboratory [5,10,35] and numerical [36] experiments. These experiments show that the diameter of a plume conduit depends on the viscosity contrast between the upwelling material and the surrounding mantle. Simulation based on realistic viscosity estimations for the upper mantle generally favor narrow conduits with diameters in the order of 100 or 200 kilometers (see e.g. [5]). This agrees well with the observation of a narrow chain of volcanic activity, 200 km wide above hotspots, attributed to melt-

ing in the plume tail [10,11]. We note however that recent numerical experiments simulating the development of axi-symmetric mantle plumes in a compressible mantle with temperature-dependent viscosity [13] suggest that broader upwelling regions may develop in the mantle.

Following a different approach, laboratory experiments conducted by Davaille [37] show that, in a chemically heterogeneous mantle, it is possible to generate hot domes with thin tubular tubes rising from their upper surfaces. These plumes could be responsible for the 'hotspots' and the domes themselves for the 'superswells' observed at the Earths's surface [37]. The anomaly we observed at 550 km depth beneath the southern part of the Red Sea could indeed be due to several narrow plume tails that we cannot distinguish because of a lack of horizontal resolution. Fig. 5 (right) and Fig. 6c show a broad low-velocity anomaly in the transition zone beneath the Red Sea, in the middle of two upwelling regions, identified from surface observations by Camp and Roobol [1] at about 12 and 23°N along the cross-section BB′ shown in Fig. 5. The first one is associated with an 'Ethiopian plume' and the other one would be located beneath the west Arabian swell. Note however that the broad low-velocity anomaly of our model is elongated in the east–west direction. This may indicate the presence at depth of plume conduits located eastward beneath the Arabian plate or the Red Sea and not on the surface location proposed by Camp and Roobol [1]. The circular anomalies we observe at 650 km depth (Fig. 6d) would support this interpretation but these latter anomalies are located at the bottom of the inverted model where the resolution is poorer. Concerning the origin of the anomalies we observe in the transition zone, recent global tomographic results [8] suggest a connection of this region with a broad low-velocity anomaly in the lower mantle. A broad upwelling zone observed in the mid-lower mantle beneath South Africa could be responsible for the uplift of the African plateau and superswell [38,39]. This anomaly is tilted by 45° in the lower mantle [8] and might provide the deep source for upwelling materials responsible for the anomaly we observe in the transition zone.

Finally, as we previously mentioned, let us recall that Nyblade et al. [14] concluded from P-to-S converted waves that the transition zone thickness beneath Afar is consistent with the global average. This is at first glance incompatible with our observation, but most of the region sampled by Nyblade et al. [14] is located southward of our deep low-velocity anomaly. In addition, they estimate the transition zone thickness with a 19 km uncertainty, consistent with a 1% low-velocity anomaly at transition zone depth. Our observation being compatible either with a broad small amplitude low-velocity anomaly or with several narrow mantle plume conduits located north of the region sampled by Nyblade et al. [14], this may explain why the transition zone thickness obtained by these authors is not affected.

For these reasons, and although we do not find a plume geometry in agreement with a simple more or less axi-symmetric broad low-velocity anomaly beneath the lithosphere overlying a unique circular conduit, we favor either a broad region of upwelling or several close narrow plume tails as an explanation for the deep low-velocity anomalies we observe beneath the southern part of the Red Sea and Arabia. A lower mantle origin of these anomalies is plausible, as suggested by several recent global tomographic studies [8].

There is a critical need for a confrontation between the plume models derived from laboratory and numerical experiments and observations from seismic tomography. This requires improvement of our seismological techniques for a better mapping of short wavelength heterogeneities in the transition zone of the upper mantle and deeper. Body-waves have up to now largely been used to detect mantle plume at large mantle depths (see e.g. [40,41]). In the upper mantle, the resolution of body-wave tomographic models is often dependent on experimental geometry near the hotspot. Several studies have shown that due to experimental geometry, it is impossible to distinguish between a shallow anomaly and a narrow deep-seated plume [42,43]. Regional tomographic techniques based on fundamental and higher mode surface waves may now provide an alternative tool for heterogeneities with a wavelength of a few hundred kilometers in the upper mantle.

Acknowledgements

References

[1] V.E. Camp, M.J. Roobol, Upwelling asthenosphere beneath western Arabia and its regional implication, J. Geophys. Res. 97 (1992) 15,255–15,271.

[2] V. Courtillot, Propagating rift and continental breakup, Tectonics 1 (1982) 239–250.

[3] P.A. Mohr, B. Zanettin, The ethiopian flood basalt province, in: J.D. Macdougal (Ed.), Continental Flood Basalts, Kluwer Academic, Boston, MA, 1988, pp. 63–110.

[4] R.G. Bohannon, C.W. Naeser, D.L. Schmidt, R.A. Zimmermann, The timing of uplift, volcanism, and rifting peripheral to the Red Sea: a case of passive rifting?, J. Geophys. Res. 94 (1989) 1683–1701.

[5] R.W. Griffiths, I.H. Campbell, Stirring and structure in mantle starting plume, Earth Planet. Sci. Lett. 99 (1990) 66–78.

[6] D.C. Almond, The relation of Mesozoic–Cainozoic volcanism to tectonics in the Afro-Arabian dome, J. Volcanol. Geotherm. Res. 28 (1986) 225–246.

[7] O. Hadiouche, N. Jobert, Geographical distribution of surface-wave velocities and 3D upper-mantle structure in africa, Geophys. J. 95 (1988) 87–109.

[8] J. Ritsema, H.J. van Heijst, J.H. Woodhouse, Complex shear wave velocity structure imaged beneath Africa and Iceland, Science 286 (1999) 1925–1928.

[9] R.B. Knox, A.A. Nyblade, C.A. Langston, Upper mantle S velocities beneath Afar and western Saudi Arabia from Rayleigh wave dispersion, Geophys. Res. Lett. 25 (1998) 4233–4236.

[10] M.A. Richards, R.A. Duncan, V.E. Courtillot, Flood basalts and hot-spot tracks: plume heads and tails, Science 246 (1989) 103–107.

[11] I.H. Campbell, R.W. Griffiths, Implications of mantle plume structure for the evolution of flood basalts, Earth Planet. Sci. Lett. 99 (1990) 79–93.

[12] G. Ito, J. Lin, C.W. Gable, Dynamic of mantle flow and melting at a ridge-centered hotspot: Iceland and the Mid-Atlantic Ridge, Earth Planet. Sci. Lett. 144 (1996) 53–74.

[13] P.F. Thompson, P.J. Tackley, Generation of mega-plumes from the core–mantle boundary in a compressible mantle with temperature-dependent viscosity, Geophys. Res. Lett. 25 (1998) 1999–2002.

[14] A.A. Nyblade, R.P. Knox, H. Gurrola, Mantle transition zone thickness beneath Afar: implications for the origin of the Afar hotspot, Geophys. J. Int. 142 (2000) 615–619.

[15] E. Debayle, J.J. Lévêque, Upper mantle heterogeneities in the Indian Ocean from waveform inversion, Geophys. Res. Lett. 24 (1997) 245–248.

[16] E. Debayle, B.L.N. Kennett, The Australian continental upper mantle: structure and deformation inferred from surface waves, J. Geophys. Res. 105 (2000) 25,423–25,450.

[17] E. Debayle, B.L.N. Kennett, Anisotropy in the Australasian upper mantle from Love and Rayleigh waveform inversion, Earth Planet. Sci. Lett. 184 (2000) 339–351.

[18] M. Cara, J.J. Lévêque, Waveform inversion using secondary observables, Geophys. Res. Lett. 14 (1987) 1046–1049.

[19] E. Debayle, SV-wave azimuthal anisotropy in the Australian upper-mantle: preliminary results from automated Rayleigh waveform inversion, Geophys. J. Int. 137 (1999) 747–754.

[20] J.P. Montagner, Regional three-dimensional structures using long-period surface waves, Ann. Geophys. 4 (1986) 283–294.

[21] O. Hadiouche, N. Jobert, J.P. Montagner, Anisotropy of the african continent inferred from surface waves, Phys. Earth Planet. Inter. 58 (1989) 61–81.

[22] C.J. Wolfe, F.L. Vernon III, A. Al-Amri, Shear-wave splitting across western Saudi Arabia: the pattern of upper mantle anisotropy at a Proterozoic shield, Geophys. Res. Lett. 26 (1999) 779–782.

[23] L.P. Vinnik, V. Farra, B. Romanovicz, Azimuthal anisotropy in the Earth from observations of *SKS* at Geoscope and NARS broadband stations, Bull. Seismol. Soc. Am. 79 (1989) 1542–1558.

[24] V. Babuška, M. Cara, Seismic Anisotropy in the Earth, Kluwer Acad., Norwell, MA, 1991.

[25] J. Trampert, J.H. Woodhouse, Global phase velocity mpas of Love and Rayleigh waves between 40 and 150 seconds, Geophys. J. Int. 122 (1995) 675–690.

[26] B.L.N. Kennett, Approximations for surface-wave propagation in laterally varying media, Geophys. J. Int. 122 (1995) 470–478.

[27] H.C. Nataf, Y. Ricard, 3SMAC: an a priori tomographic model of the upper mantle based on geophysical modeling, Phys. Earth Planet. Inter. 95 (1995) 101–122.

[28] H. Marquering, R. Snieder, G. Nolet, Waveform inversion and the significance of surface-wave mode coupling, Geophys. J. Int. 124 (1996) 258–278.

[29] J. Ritsema, H.J. van Heijst, New seismic model of the upper mantle beneath Africa, Geology 28 (2000) 63–66.

[30] D.A. Griot, Tomographie anisotrope de l'Asie centrale à partir d'ondes de surface, Ph.D. thesis, Université Paris VII, Paris, 1997.

[31] W.D. Mooney, G. Laske, G. Masters, Crust5.1: a global crustal model at 5×5, J. Geophys. Res. 103 (1998) 727–747.

[32] D.L. Anderson, T. Tanimoto, Y. Zhang, Plate tectonics and hotspots: the third dimension, Science 256 (1992) 1645–1651.

[33] D.L. Anderson, The sublithospheric mantle as the source of continental flood basalts; the case against the continental lithosphere and plume head reservoirs, Earth Planet. Sci. Lett. 123 (1994) 269–280.

[34] S.D. King, J. Ritsema, African hot spot volcanism: small-scale convection in the upper mantle beneath cratons, Science 290 (2000) 1137–1140.

[35] J.A. Whitehead, D.S. Luther, Dynamics of laboratory diapir and plume models, J. Geophys. Res. 80 (1975) 705–717.

[36] G.F. Davies, Penetration of plates and plume through the mantle transition zone, Earth Planet. Sci. Lett. 133 (1995) 507–516.

[37] A. Davaille, Simultaneous generation of hotspots and superswells by convection in a heterogeneous planetary mantle, Nature 402 (1999) 756–760.

[38] A.A. Nyblade, S.W. Robinson, The African superswell, Geophys. Res. Lett. 21 (1994) 765–768.

[39] M. Gurnis, J.X. Mitrovica, J. Ritsema, H.J. van Heijst, Constraining mantle density structure using geological evidence of surface uplift rates: the case of the African superplume, Geochem. Geophys. Geosyst. 1 (2000) 1999GC000035.

[40] Y. Ji, H.C. Nataf, Detection of mantle plumes in the lower mantle by diffraction tomography: Hawaii, Earth Planet. Sci. Lett. 159 (1998) 99–115.

[41] H. Bijwaard, W. Spakman, Tomographic evidence for a narrow whole mantle plume below Iceland, Earth Planet. Sci. Lett. 166 (1999) 12–126.

[42] R.L. Saltzer, E.D. Humphreys, Upper mantle P-wave velocity structure of the eastern Snake River plain and its relationship to geodynamic models of the region, J. Geophys. Res. 102 (1997) 11829–11841.

[43] W.R. Keller, D.L. Anderson, R.W. Clayton, Resolution of tomographic models of the mantle beneath iceland, Geophys. Res. Lett. 27 (2000) 3993–3996.

[44] P. Wessel, W.H.F. Smith, New version of the generic mapping tools released, EOS Trans. Am. Geophys. Union 76 (1995) 329.